Optical Metasurfaces and Prospect of Their Applications Including Fiber Optics

Nanfang Yu, *Member, IEEE*, and Federico Capasso, *Fellow, IEEE*

(Invited Tutorial)

***Abstract*—Metasurfaces have emerged in the recent years as a platform to design subwavelength-thick optical components ("flat optics"), which can be used to implement any optical function (beam deflection, focusing, waveplates, etc). These flat optical components can be fabricated using a single lithographic step. The approach is particularly suited for patterning nonconventional substrates, such as semiconductor laser facets and optical fiber facets. In this paper, we review recent applications of metasurfaces to flat optical devices, including their use in semiconductor lasers and fiber optics. Metasurfaces make it possible to design all properties of light (amplitude, phase, and polarization), which enable us to build a large variety of flat optical components, including planar lenses, quarter-wave plates, optical vortex plates, holograms for vector beam generation, and ultrathin perfect absorbers and color coatings. We also review flat collimating lenses integrated on the facets of mid-infrared and far-infrared (terahertz) quantum cascade lasers, and novel techniques to create large arrays of nanostructures on fiber facets.**

***Index Terms*—Antenna arrays, metasurfaces, optical fibers, optical surface waves, phased arrays, quantum cascade lasers.**

I. Introduction

METASURFACES are powerful ways to realize transformation optics [1]–[4]. By introducing abrupt phase shifts, they allow us to fold optical space at the interface between two optical media (i.e., optical analog of origami), so that we can control light transmitted through, reflected from, or propagating along a designer optical interface [5]–[9]. This paper will address the question of how the emerging technology of metasurfaces can leverage the strength of fiber optics, which is a powerful and well-established technology platform.

Manuscript received November 20, 2014; accepted December 8, 2014. Date of publication February 18, 2015; date of current version April 29, 2015. This work was supported by the National Science Foundation under Grant ECCS-1307948, the Harvard Nanoscale Science and Engineering Center under contract NSF/PHY 06-46094, and the Center for Nanoscale Systems at Harvard University, which is a member of the National Nanotechnology Infrastructure Network and also supported in part by the Defense Advanced Research Projects Agency (DARPA) N/MEMS S&T Fundamentals program under Grant N66001-10-1-4008 issued by the Space and Naval Warfare Systems Center Pacific and by the Air Force Office of Scientific Research under Grant FA9550-12-1-0289. The work of N. Yu was supported by the Fu Foundation School of Engineering and Applied Science, and the Department of Applied Physics and Applied Mathematics, Columbia University.

N. Yu is with Department of Applied Physics and Applied Mathematics, Columbia University, New York, NY 10027 USA (e-mail: ny2214@columbia.edu).

F. Capasso is with School of Engineering and Applied Sciences, Harvard University, Cambridge, MA 02138 USA (e-mail: capasso@seas.harvard.edu).

Color versions of one or more of the figures in this paper are available online at http://ieeexplore.ieee.org.

Digital Object Identifier 10.1109/JLT.2015.2404860

We will review the basic physics and applications of metasurfaces. We have always been interested in the opportunities that plasmonics and metasurfaces can bring to the field of fiber optics. In this regard, we will describe our previous effort in developing nonconventional methods to pattern optical fiber facets with arrays of nanostructures. There are certain similarities between the optical fiber platform and the semiconductor laser platform. We believe that some of the key concepts developed through our work on engineering the wavefront of semiconductor lasers using plasmonic structures can be adapted to the fiber optics platform. Therefore, we will also review a selection of examples on controlling laser near-field and far-field using plasmonics.

II. Basic Concept of Metasurfaces and Their Applications

A. Wavefront Control With Metasurfaces

The essence of metasurfaces is to use arrays of antennas with subwavelength separation and with spatially varying geometric parameters (e.g., antenna shape, size, orientation) to form a spatially varying optical response, which molds optical wavefronts at will [5]–[9]. Metasurfaces allow us to mold light propagation using phase discontinuities (defined as abrupt changes of phase over a distance comparable to the wavelength). We can directly engineer the phase, amplitude and polarization along the surface using optical resonators so that we can make a new class of optical components. In this sense, the refractive index is a not a particularly useful quantity to characterize metasurfaces.

We have many choices to create abrupt optical phase shifts. Any type of optical resonators can be used, including plasmonic antennas [10], [11], dielectric resonators [12]–[14], quantum dots, and nano-crystals. The optical resonators, however, have to satisfy the following requirements: they should have subwavelength thickness; they must have small footprints so that they can be packed together with subwavelength separations; their phase response should cover the entire 2π range; and the scattering amplitude must be uniform and large across the array. Plasmonic antennas are basically metallic nanoparticles. In the case of simple metallic nanorods, if the wavelength is fixed, the variation of the length of the rod will introduce a shift in the phase of the scattered light. The phase shift is actually significant: it can approach π for very conductive thin rods [15]. We are conceptually in the context of transmit-arrays and reflect-arrays that have been studied by the microwave and mm-wave community [16]–[18]. For example, the famous Yagi-Uda antenna

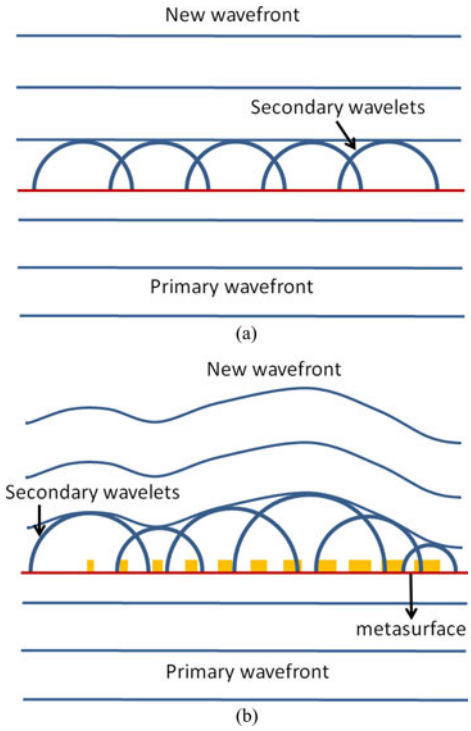

Fig. 1. Schematics showing Huygens' principle applied to a flat non-structured surface (a), and a metasurface (b) Note that in these diagrams, we assume that the two optical media are impedance matched, so that there are only optical scatterings in the forward direction.

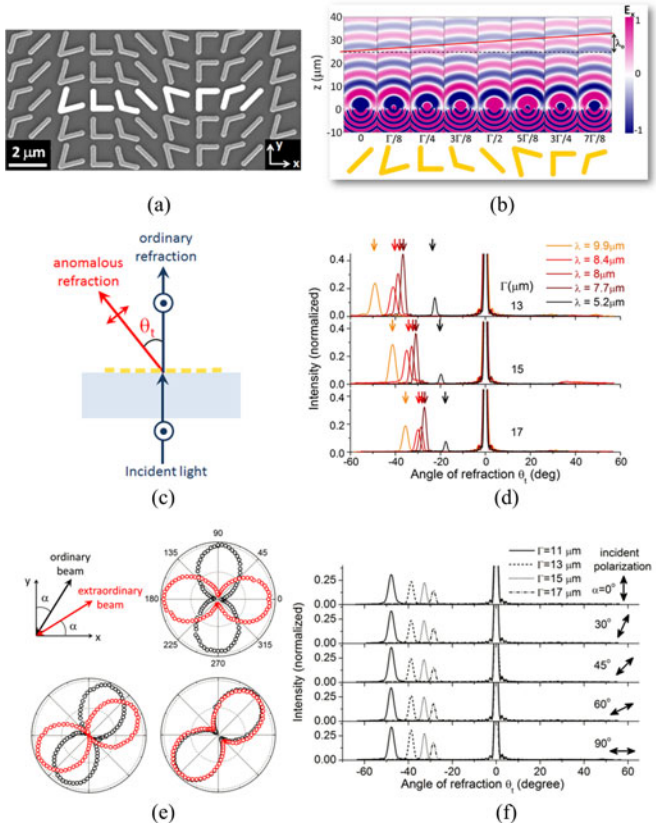

Fig. 2. (a) SEM image of a metasurface consisting of a phased optical antenna array fabricated on a silicon wafer. The metasurface introduces a linear phase distribution along the interface and is used to demonstrate the generalized laws of reflection and refraction. The unit cell of the structure (highlighted) comprises eight gold V-antennas of width ~220 nm and thickness ~50 nm and it repeats with a periodicity of $\Gamma = 11$ μm in the horizontal direction and 1.5 μm in the vertical direction. (b) FDTD simulations of scattered electric field for individual antennas. (c) Schematic of the experimental setup. (d) Experimental far-field scans showing the ordinary and extraordinary refraction generated by metasurfaces with different interfacial phase gradients (from $2\pi/13$ to $2\pi/17$ μm^{-1}) at different wavelengths (from 5.2 to 9.9 μm), given normally incident light. (e) Schematics showing the polarizations of the ordinary and extraordinary beams generated from the metasurface in (a). Measured intensity of the ordinary and extraordinary beams, represented by black and red circles, respectively, as a function of the rotation angle of a linear polarizer in front of the detector for different incident polarizations: $\alpha = 0°$, 30°, and 45°. (f) Far-field scans of transmitted light through the metasurface in (a). Plane-wave excitations at $\lambda = 8$ μm with different polarizations were used and four samples with different period Γ were tested.

achieves beam shaping based on the principle that a variation of the length of antenna rods gives rise to controllable phase response [19]–[21]. However, the wavelengths we are working on are orders of magnitude shorter, which can bring forth significantly interesting new physics and will have impact on completely different technological areas.

Metasurfaces are certainly related to diffractive optics [22]. The merit of metasurfaces is the technological simplification: metasurfaces allow one to use a single-digital pattern (i.e., one lithographic mask) to create an arbitrary analogue optical phase response (e.g., amplitude, phase, polarization, and optical impedance). So far most of the metasurface structures are fabricated using electron-beam lithography, but manufacturing techniques for large-scale patterning of planar structures are available, such as nano-imprint lithography [23], soft lithography [24], and deep-UV lithography [25], [26].

The physics of metasurfaces can be understood in terms of Huygens' principle: every point on an interface creates a spherical wavelet, and the interference of the wavelets forms the new wavefront. For a regular non-structured surface, normal incident light passes through without changing the propagation direction. However, for an inhomogeneous interface, made of a distribution of resonators, dissimilar in their scattering properties, the wavefront will be molded according to the phase response of the resonators (see Fig. 1). To study the phenomena of reflection and refraction of light from such metasurfaces, we can apply Fermat's principle, which states that the path of light should have stationary phase (i.e., two infinitesimally close paths should have optical phase difference of zero). These optical paths consist of both propagation phase and phase jumps at the interface. The generalized laws of reflection and refraction can be derived by imposing the stationary phase condition on the so-called "gradient metasurface", which introduces a constant phase gradient along the interface. As a result, in addition to the ordinary terms in the Snell's law and law of specular reflection, the generalized laws contain a term proportional to the phase gradient [5]. A simple way to interpret the generalized law is the conservation of wavevector along the interface: the metasurface impacts to the scattered beams (refracted and reflected beams) a wavevector equal to the phase gradient [27].

Fig. 2(a) shows a scanning electron microscope (SEM) image of the first metasurface we demonstrated, which is basically a phased array antenna in the mid-infrared (mid-IR) [5]. We

used the metasurface to demonstrate the generalized laws of reflection and refraction. The building block of the metasurface is the row of antennas highlighted in Fig. 2(a). These are V-shaped antennas that have subwavelength thickness of 50 nm. The antennas have uniform scattering amplitude but linearly varying phase response: from the first to the last element in the array, the phase of the scattered light changes from 0 to $7\pi/4$ in steps of $\pi/4$. The advantages of the metasurface are multifold: they allow for instant molding of optical wavefronts; they are easy to fabricate; they have greatly reduced device size and weight compared to bulky optical components; and they allow for engineering the near-field, meso-field, and far-field of optical waves. Fig. 2(b) shows how the scattered wavelets from each antenna look like, assuming that the antennas are illuminated by an incident wave coming from inside the silicon substrate. The envelope of the wavelets defines the new wavefront according to Huygens' principle and we see that the wavefront is tilted because of the phase gradient introduced by the metasurface.

We would like to elaborate a bit on the physics of V-antennas. V-antennas are not new; they were used in Sputnik satellite and old TV sets. Zheludev *et al.* analyzed the symmetry properties of these V-antennas [28]. V-antennas allow for a versatile manipulation of the amplitude and phase of light and they are inherently broadband. The antennas support a symmetric mode of the oscillation of the current and an antisymmetric mode [29], [30]. There is a factor of two difference in the relevant length of the two modes so that the two modes are shifted by approximately a factor of two in their resonant wavelengths. The resonant modes can be treated as harmonic oscillators that reradiate or scatter light [29], [30]. It is very important to recognize that to shape the far-field, we should use optical resonators with low quality factors, because the resonators must have high radiative losses [31]. The presence of two eigen-modes in a single optical resonator allows us to achieve polarization conversion, which is a convenient method to obtain the 2π phase modulation necessary for the complete control of the wavefront. In our initial experiments, we chose an incident polarization such that both the symmetric and antisymmetric modes can be excited. The scattered light was a linear combination of the fields produced by the eigenmodes, and we only captured the scattered light polarized normal to the incident field. We were able to vary the phase of the scattered light from 0 to π by changing the length of the antenna arms and the angle between the two arms. To cover an additional π range, we used the mirror structures where the horizontal components of the oscillating current in the antennas were flipped, which created scattered waves with an extra π phase shift.

Fig. 2(d) shows experimental results at normal incidence. The far-field measurements showed that the polarization of the anomalous refraction is rotated 90° compared to that of the incident light. There was still ordinary (zeroth-order) diffraction, which has the same polarization as the incident light and propagates normal to the metasurface. The metasurface functionally acts like a blazed grating; it uses phase discontinuities to create only one diffraction order, whereas conventional blazed gratings rely on the propagation phase. Note, however, blazed gratings are narrowband. Fig. 2(d) shows that the metasurface is broadband. It creates anomalous refraction from about 5 to 10 μm in wavelength [6]. We have studied the metasurfaces with incident light of different polarizations (Fig. 2(e) and (f)). If the incident light has a polarization not exactly 45° from the axis of the symmetric and antisymmetric modes of the antenna, the anomalous refraction will not be cross-polarized [6]. The angle of refraction is still given rigorously by the generalized law of refraction.

The efficiency of a metasurface depends on the design. The efficiency of our metasurfaces made of a single layer of structured metal is not too high, and there are three reasons: (1) there is polarization conversion, (2) optical power is divided between reflected and refracted beams, and (3) the antenna array has a finite filling factor. The filling factor can be improved. For example, one can use the mutual coupling between the antennas. But, fortunately, there are other strategies that allow for a considerable increase of the scattering efficiency and will be discussed in the following paragraphs.

Our initial work was generalized by the Shalaev group in the near-infrared wavelength range, where they showed broadband light bending from $\lambda = 1$ to 2 μm [32]. Research groups from Fudan University and National Taiwan University were the first to address the issue of efficiency. They studied gradient metasurfaces based on reflect-arrays at the visible, near-infrared, and microwave wavelengths [33], [34]. The idea was to place a metal sheet with a subwavelength distance from the layer of optical scatterers. This approach cancels the transmitted beams and therefore enhances the intensity of the reflected beams. But more importantly, even though simple antennas were used as the optical scatterers, because of their near-field interaction with the metal sheet (the antennas induce anti-parallel currents in the metal sheet through near-field coupling), 2π phase modulation can be achieved.

Metasurfaces based on reflect-arrays were initially studied by a research group from Fudan University in the microwave spectral range [34]. They used H-shaped antennas with varying sizes. They studied beaming of the anomalously reflected light. In particular, by choosing the incident angle and designing the phase gradient properly, they could redirect 95% of the incident power into the anomalous reflection channel. They also demonstrated that there is a critical angle above which there is no anomalous reflection: all the incident optical power is coupled into surface waves. They used microwave scanning probes to characterize the generated surface waves. These surface waves are short lived and got absorbed quickly by the metasurfaes, because there are no eigen surface modes in the gradient metasurfaces. The significance is that these are really new surface waves (very different from surface plasmon polaritons on flat metal-dielectric interfaces) because the metasurface is spatially inhomogeneous.

A similar concept was demonstrated in the near-infrared around $\lambda = 800$ nm by the group from National Taiwan University [33]. They used simple rod antennas with varying lengths. The near-field coupling between the rods and their dipolar images in the back metal sheet allowed for a full 2π phase coverage. They demonstrated experimentally that the anomalous reflection mode can take as much as 80% of the incident power.

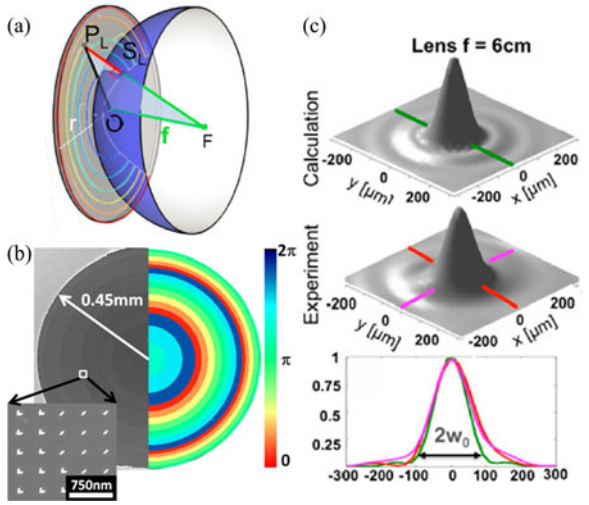

Fig. 3. (a) Schematic showing the design of a metalens. In order to focus a plane wave to a single point at distance f from the lens, a hyperboloidal phase profile must be imparted onto the incident wavefront to compensate for the difference in propagation phase. (b) Left: SEM image of a fabricated planar lens with 3-cm focal length consists of an array of V-antennas. Right: Phase profile of the lens discretized according to the phase responses of eight constituent antennas. Inset: Zoom-in view of fabricated antennas. The antenna array has a square lattice with a lattice constant of 750 nm. (c) Calculated and measured intensity distribution of the lens (b) on the focal plane.

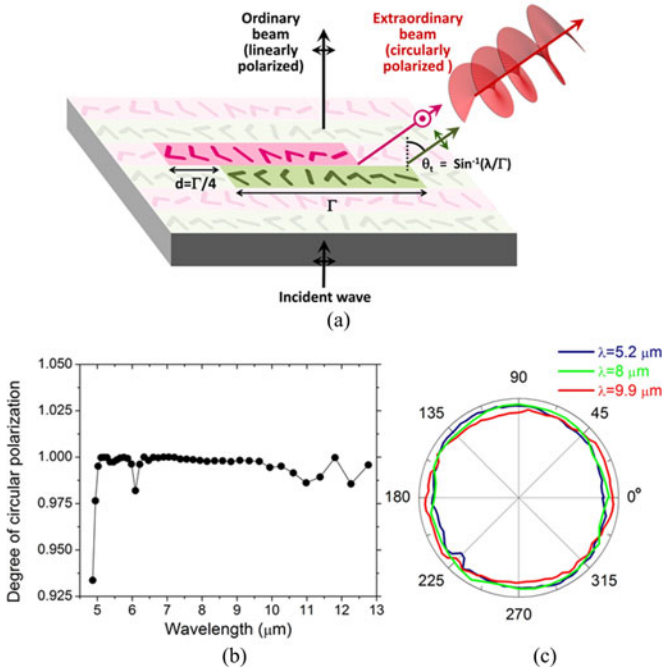

Fig. 4. (a) Schematics showing the working mechanism of a metasurface quarter-wave plate. The unit cell of the metasurface consists of two sub-units each containing eight gold V-antennas. Upon excitation by linearly polarized incident light, the sub-units generate two copropagating waves with equal amplitudes, orthogonal linear polarizations, and a $\pi/2$ phase difference (when offset $d = \Gamma/4$), which produce a circularly polarized extraordinary beam that bends away from the surface normal. The metasurface also generates an ordinary beam propagating normal to the surface and with the same polarization as the incident light. (b) Calculated degree of circular polarization of the extraordinary beam as a function of wavelength. (c) State-of-polarization analysis for the extraordinary beam at $\lambda = 5.2$, 8, and 9.9 μm. The measurements are performed by rotating a linear polarizer in front of the detector and measuring the transmitted power.

B. Flat Optical Components Based on Metasurfaces

1) Metalens: We will first describe a metalens [35] based on metasurfaces (see Fig. 3). The metalens is a flat lens that allows one to create a spherical wavefront when incident light with a flat wavefront impinges on the metasurface in the normal direction. The scattered wavefront is rigorously spherical; therefore, there is no spherical aberration (under normal incidence). The metalens consists of arrays of optical scatterers. To create a spherical wavefront, the total accumulated phase, including propagation phase and phase jumps due to optical scattering, has to be the same from every point on the metalens to the focal point of the lens. The propagation distance from outer regions of the lens to the focal point is longer; therefore, the metalens was designed to compensate for the propagation phase shift by decreasing the abrupt phase shift due to scattering in the outer regions of the lens. We have shown that the spatial distribution of the phase jumps has to follow a hyperboloidal function. The metalens eliminates spherical aberration, making it possible to realize high numerical aperture. However, it does not compensate for comatic aberration. We have shown in a later work that if one let the metasurface have some curvature, the comatic aberration can be significantly reduced [36]. Our demonstrated metalenses suffer from the problem of efficiency. The groups of Andrea Alú and Anthony Grbic have shown that metalenses with three layers of optical scattering elements can substantially enhance the transmission efficiency of optical power [37], [38].

2) Quarter-Wave Plates: We demonstrated a broadband quarter-wave plate [39] based on metasurfaces (see Fig. 4). The unit cell of the metasurface waveplate contains two sub-units, which create two linearly-polarized field components with the same amplitude, orthogonal polarizations, and a phase shift of 90° in order to create a circularly polarized wave. To get the 90° phase shift between scattered waves from the sub-units, we slide the two sub-units from each other by a quarter of the length of the unit cell. We have shown experimentally that the waveplates work from 5 to 12 μm wavelength generating a beam with circular polarization of high purity (intensity ratio between the wanted and unwanted circular polarization over 400 from $\lambda = 5$ to 12 μm). The metasurface waveplate works for arbitrary linear incident polarization and it is background free: the ordinary transmitted beam is separated from the circularly-polarized anomalously refraction.

3) Vortex Plates: We have used metasurfaces to create non-conventional beams such as optical vortex beams (see Fig. 5). An optical vortex has a spiral wavefront; the optical power (Poynting vector) spirals around the propagation direction and therefore carries orbital angular momentum (OAM) [40], [41]. The order of such OAM is determined by the number of twists of the wavefront with in a propagation distance of one wavelength. The phase is indetermined at the center of the beam. As the order of OAM increases the region of zero intensity at the center of the beam increases. Optical vortices have been conventionally created using spiral phase plates, fork-shaped gratings, or spatial light modulators.

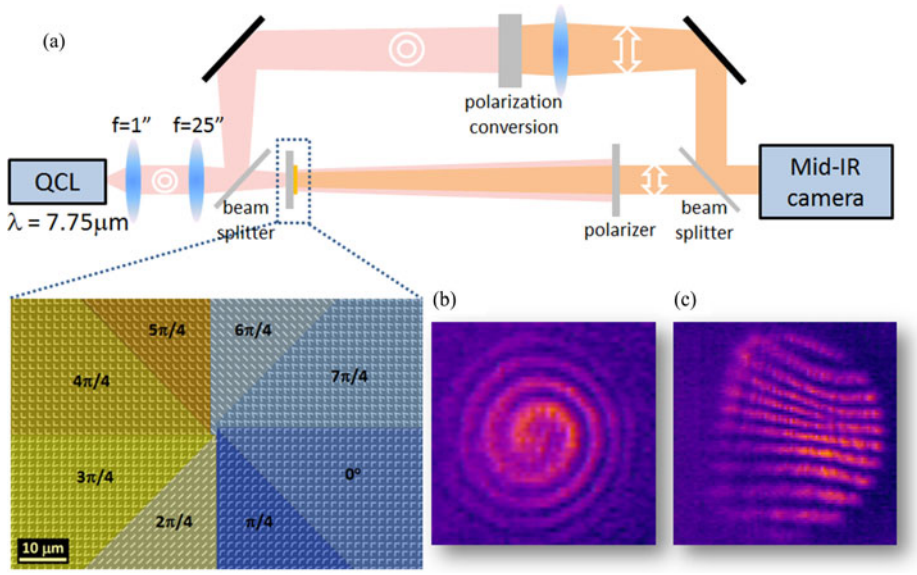

Fig. 5. (a) Experimental setup based on a Mach–Zehnder interferometer used to generate and characterize optical vortices. The inset is an SEM image showing a metasurface phase plate corresponding to the first-order optical angular momentum. The antennas are arranged to generate a phase shift that varies azimuthally from 0 to 2π, thus producing a helicoidal scattered wavefront. (b) Spiral interference pattern created by the interference between a vortex beam and a copropagating Gaussian beam. (c) Interference pattern with a dislocated fringe created by the interference between a vortex beam and a plane wave intersecting at a small angle.

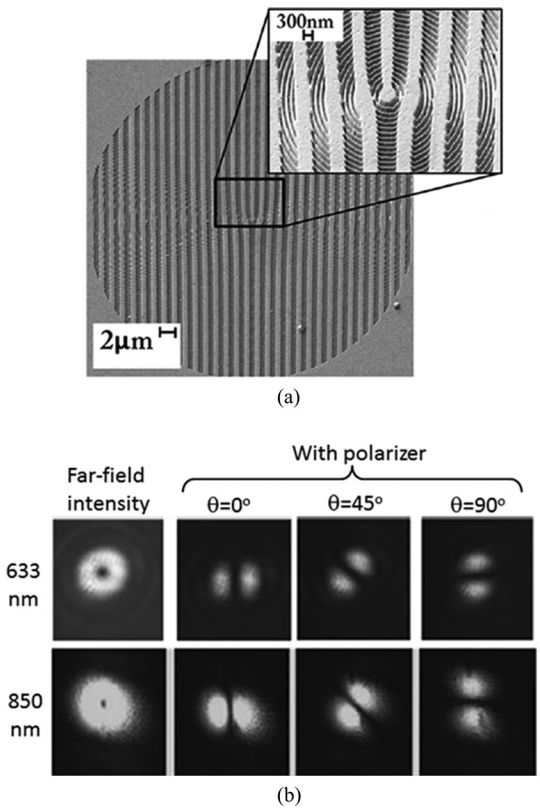

Fig. 6. (a) SEM image of the fork holographic metasurface. (b) Measured far-field intensity distributions at two wavelengths, without and with analyzer. These intensity patterns demonstrate that the first-order diffracted beam from the fork hologram is radially polarized and that the device is broadband.

We used a metasurface to impart OAM to the incident beam [5], [42]. The metasurface was created by assembling an array of V-antennas so that in the azimuthal direction the phase response increases linearly from 0 to 2π (for first order OAM). Experiments were done using mid-infrared QCLs as the light source. If there was no reference beam, the cross-section of optical vortices taken using an infrared camera showed a donut; if the reference beam and the optical vortex beam were collinear, we obtained a spiral interference pattern; if the two beams intersected each other at a small angle, we obtained a set of interference fringes with a dislocated fringe at the center (for first order OAM). The molding of optical wavefront by the metasurface is abrupt: we showed in full-wave simulations that fully formed optical vortices are created within a subwavelength distance from the metasurface [6].

Initial work on metasurfaces used the dispersion of antennas to realize phase control. But there is a completely different way to achieve abrupt phase changes. The new approach is based on the so-called Pancharatman–Berry (PB) phase [43], [44], which is the phase change related to the variation of optical polarization. In one implementation of the PB phase, tiny apertures of the same shape but with different orientation directions were used. These apertures can be treated as tiny polarizers. Calculations based on Jones matrix formulation showed that the transmission through the aperture contains a phase that is determined by the orientation of the aperture, as well as the handedness of the incident circular polarization [45]. A variety of flat optical components have been created based on metasurfaces made of arrays of dielectric ridges, apertures defined in metal films, or metallic rods; these include metalenses that focus circularly polarized light, and plates that generate optical vortices [46]–[51]. The major advantage of building flat optics using PB phase is that the metasurface devices can operate over a broad wavelength range, because the phase distribution originates from the spatial orientation of the optical scatterers, instead of antenna dispersion. The metasurfaces based on PB phase are thus dispersionless.

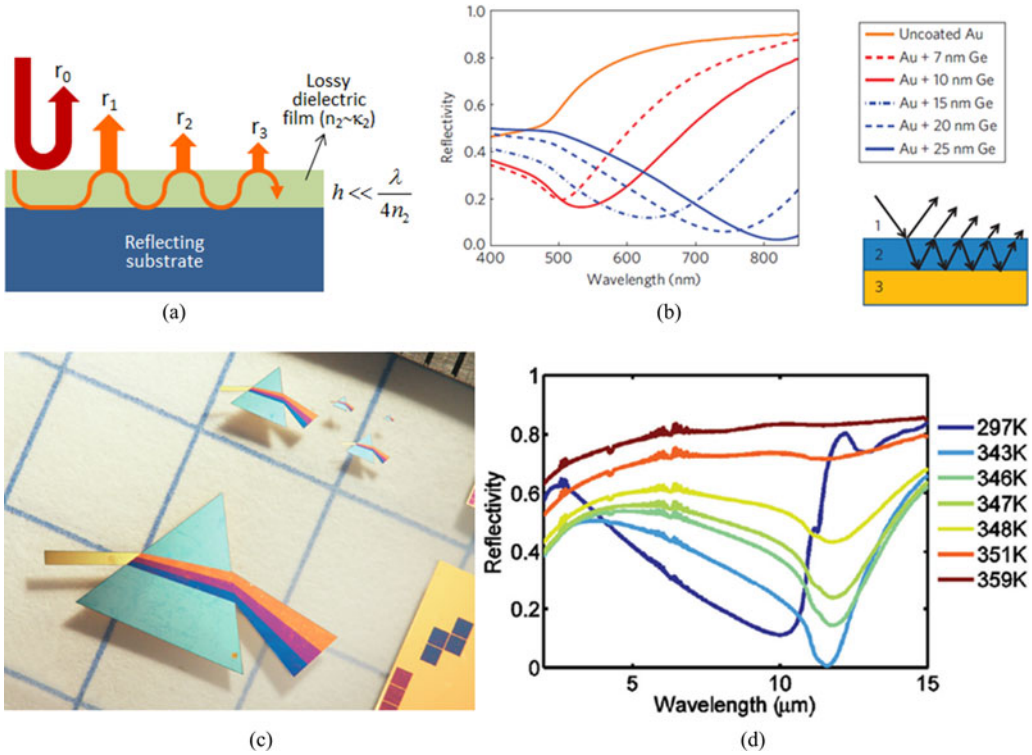

Fig. 7. (a) Schematic showing the reflection process from a highly absorbing ultrathin film on a lossy substrate. (b) Reflection spectra of ultra-thin germanium films of different thicknesses deposited on gold. (c) Photograph of color images generated using multistep patterning of ultrathin germanium films. Five steps of photolithography with alignment are used to selectively deposit an optically thick layer of Au on a glass slide, followed by Ge layers of 7, 11, 15 or 25 nm, yielding light pink, purple, dark blue and light blue colors, respectively. (d) Experimental reflection spectra of a sample consisting of a sapphire substrate coated with 180 nm of vanadium dioxide (VO_2) at temperatures from 297 to 359 K. Maximum absorption (reflectivity ~0.0025) is reached at $\lambda = 11.6\ \mu$m at 343 K.

4) Holograms for Vector Beam Generation: Recently, we have demonstrated a holographic flat optical element that can locally change not only the phase and amplitude but also the polarization of light over a broad wavelength range [52]. The metasurface was made of a superposition of a fork grating and an array of concentric grooves with subwavelength separations (see Fig. 6(a)). When illuminated by a circularly polarized beam, the metasurface generated a pair of diffracted beams, which had spiral wavefronts and radial polarization (see Fig. 6(b)).

5) Metasurfaces Based on Ultra-Thin Films: Thin-film interference in optical coatings introduces useful functionalities such as anti-reflectivity, high-reflectivity, spectral filtering and beam-splitting. Optical coatings are used in almost every optical systems, but they are almost ubiquitously based on low-loss dielectric films: the film thicknesses are at least on the order of the wavelength of light. Optical losses are considered detrimental because they reduce the number of partial waves that can participate in the desired constructive or destructive interference.

We studied a very different scheme of thin-film interference [53]–[55], where the films are made of highly absorbing materials but are significantly thinner than one wavelength of light, so that the light is not completely attenuated in a single pass in the film and multi-beam interference is still possible (see Fig. 7(a)).

In lossless dielectric films, optical phase is accumulated via propagation: the reflection at an interface merely contributes a phase jump of 0 or π. However, when the film has a significant imaginary part of the complex refractive index, the reflection coefficient dictated by Fresnel equations takes complex values. Therefore, the phase acquired upon reflection at the boundary of lossy materials can have any value between 0 and π, which means that an optically thin film can act effectively like a thick film.

Our first demonstration of ultra-thin-film interference used amorphous germanium as the lossy material, which was deposited on a gold substrate (see Fig. 7(c)) [55]. This structure allows for enhanced absorption in the visible through destructive interference between reflected partial waves. Experiments showed that germanium films with thickness between 5 and 25 nm exhibit colors varying from pink to blue (see Fig. 7(c)). The spectral shift is approximately 20 nm in wavelength per 1nm change of the film thickness, and the enhanced absorption can be up to 80% of the incident light (see Fig. 7(b)). One important feature of the ultra-thin-film interference is that the coloration of the film is not sensitively dependent on the viewing angle; therefore, the ultra-thin interference coatings appear optically like a thin film of paint.

In a second demonstration, we used a phase change material vanadium dioxide (VO_2) deposited on a sapphire substrate [53], [54]; both have complex refractive indices in the mid-IR spectral range. The optical conductivity of VO_2 undergoes a dramatic change at its phase transition temperature (~65 °C) [56]. At low temperatures, VO_2 is almost transparent in the mid-IR, whereas at high temperatures VO_2 is a lossy metal. At an intermediate temperature, however, VO_2 is neither a

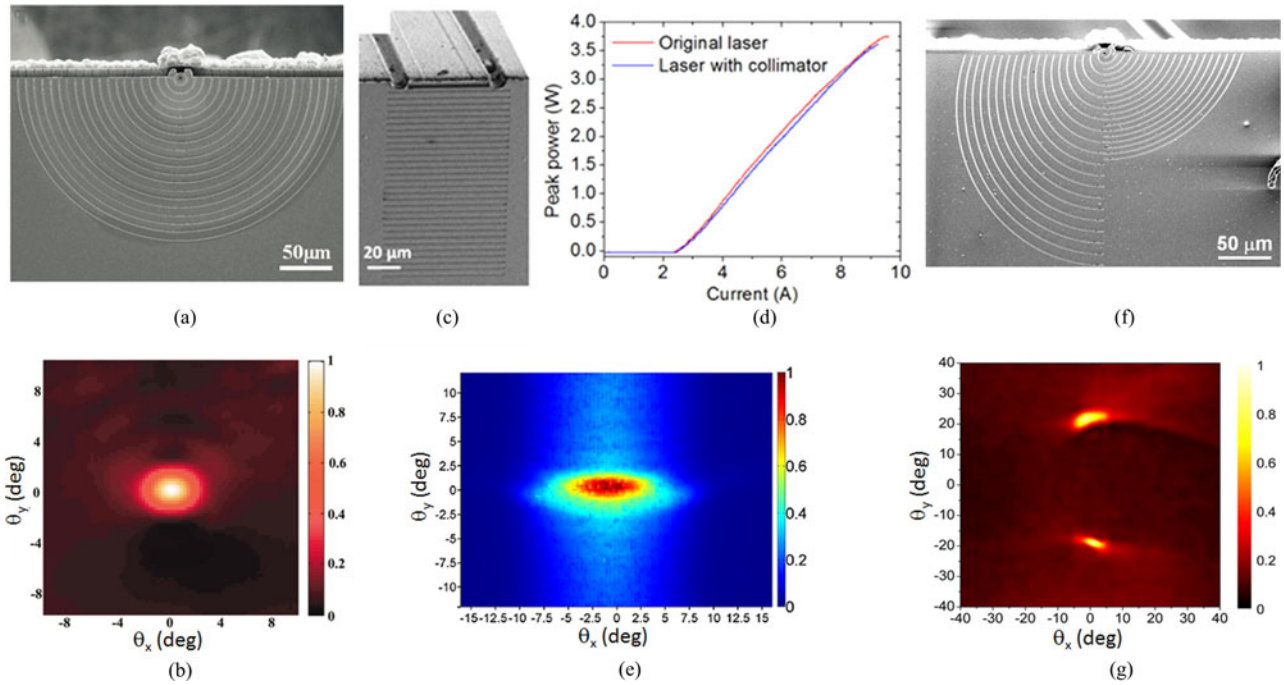

Fig. 8. (a) SEM image of a $\lambda = 8.1$ μm QCL integrated with a 2-D plasmonic collimator (aperture size 2×2 μm^2). (b) Measured emission pattern of the device in (a). (c) SEM image of a $\lambda = 8.1$ μm wide-ridge QCL integrated with a 1-D plasmonic collimating lens. (d) LI curve of the device shown in (c), taken before and after fabrication of the collimator. Both the collimated beam and a residual uncollimated background are measured. (e) Two-dimensional far-field intensity distribution of the device shown in (c), measured using a microbolometer array. (f) SEM image of a $\lambda = 8.1$ μm QCL patterned with two elliptical collimating lenses. (g) Measured emission pattern of the device in (f).

dielectric nor metal (microscopically, it is a percolation of metal nanostructures in a dielectric matrix; optically, the real part of the complex refractive index is comparable to the imaginary part). We observed in experiments that the reflectivity drops to zero around 12 μm wavelength (see Fig. 7(d)), corresponding to complete destructive interference between reflected partial waves. The phenomenon could be exploited to enhance light absorption in thin film optoelectronic devices, such as solar cells, water-splitting cells, and designer thermal radiators [57].

III. Wavefront Engineering of Semiconductor Lasers Using Plasmonic and Metasurface Structures

We have been working on wavefront engineering of semiconductor lasers extensively for a number of years [58], [59]. By patterning the laser facets with properly designed planar plasmonic structures, we were able to engineer the optical near-field and far-field of laser emission. In particular, we have experimentally demonstrated a few useful device functionalities, including concentrating laser emission into a subwavelength spot on the laser facet, collimation of laser beams, controlling of laser polarization, and beaming of laser emission into arbitrary directions [60]–[70]. Many concepts and techniques we have developed to control laser emission can be adapted for controlling light emission from an optical fiber facet, because in both systems light propagation is confined in optical waveguides.

A. Plasmonic Collimators for the Mid-Infrared Spectrum

Fig. 8(a) shows a mid-infrared quantum cascade laser integrated with a flat collimating lens, which consists of a rectangular subwavelength aperture and a circular plasmonic second-order grating on the laser facet [63], [64]. The key to reduce the divergence of laser beam in the far-field is to spread the optical power over an area as large as possible in the near-field. The subwavelength aperture couples a substantial portion of the laser emission into surface waves propagating in two dimensions on the laser facet. The optical power is then progressively scattered into the free space by scatterers distributed on the laser facet. The laser far-field is then the coherent superposition of the scattered waves from the aperture and from the scatterers. Since the wavefront of surface waves propagating on laser facet in this case is circular, we used a circular grating as the scattering element. We demonstrated experimentally 2-D collimation using QCLs provided by Hamamatsu. The divergence angle of the laser beam was reduced by more than one order of magnitude from tens of degrees to only a few degrees in both the vertical and horizontal directions (see Fig. 8(b)). The output power of the laser, however, decreased considerably (i.e., about 20% of the original laser). The reduction of optical power is not because of optical losses in the metallic collimating lens (in the mid-IR wavelength range the plasmonic losses are limited); it is because the subwavelength aperture does not permit efficient optical transmission.

In a later experiment, we demonstrated collimated, Watt-level laser output from QCLs with tapered waveguides and patterned with 1-D plasmonic collimating lenses (see Fig. 8(c)) [70]. The laser waveguide consists of a 0.5 mm-long and 14 μm-wide narrow ridge section, followed by a 2.5 mm-long tapered section with a 1-degree half-angle, so that the waveguide has a width about 100 μm on the facet (see Fig. 8(c)). We widened the

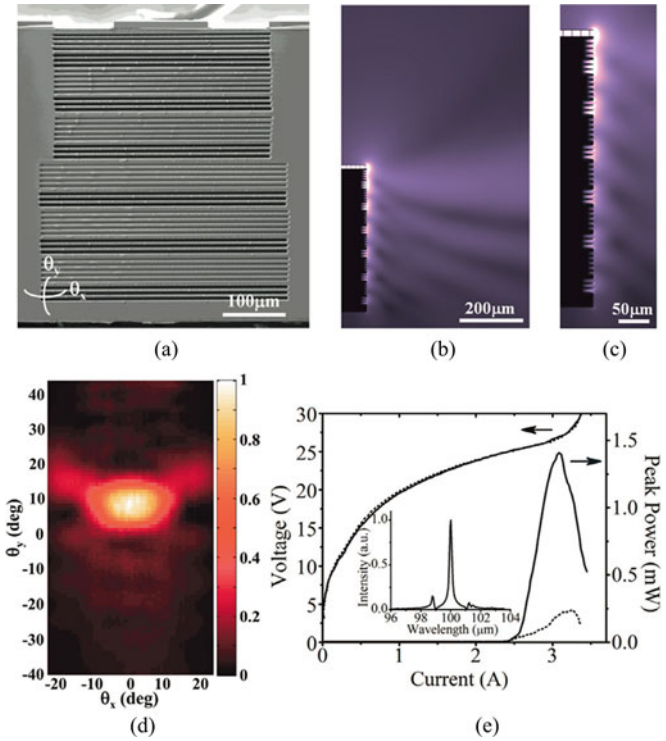

Fig. 9. (a) SEM image of a THz QCL integrated with a metasurface collimator. The laser emission wavelength is 100 μm and it has a 1.2-mm-long, 150-μm-wide, and 10-μm-thick waveguide. (b) Simulated electric-field distribution (|E|) of the collimated device. (c) Zoom-in view of (b). (d) Measured far-field intensity distributions of the collimated device. (e) *L–I–V* characteristics of the device. The dotted and solid curves are for the original unpatterned device and the device with the metasurface collimator, respectively. Inset: emission spectrum of collimated device at a pump current of 3A.

aperture so that it has a dimension similar to the laser waveguide. The two-dimensional far-field profile of the collimated laser is shown in Fig. for a driving current of $\mathrm{I} = 3.5\mathrm{Ith}$. We observe that the collimator results in a central low-divergence beam with FWHM of 7.5° and 3°, respectively, along the horizontal and vertical directions (see Fig. 8(e)). The optical power output of the collimated laser was very similar to that of the original laser (see Fig. 8(d)). We have made a more complex collimator, which consists of arrays of elliptical grooves and can produce multiple laser beams propagating at arbitrary angles with respect to the axis of the laser waveguide (see Fig. 8(f) and (g)).

B. Metasurface Collimators for the Far-Infrared Spectrum

Terahertz QCLs ($\lambda = 60$–300 μm) based on double-metal waveguides have the highest operating temperature [71]. The laser waveguide mode is squeezed between two metal plates and the laser beam is strongly diffracted at the waveguide ends, which are basically subwavelength apertures. Our first attempt to collimate the laser beam was to mill a set of second-order grating grooves on the cleaved laser substrate, which is made of heavily doped GaAs, a plasmonic material in the THz frequency range. The method did not work very well because a lot of optical power was still scattered into directions not normal to the laser facet. The reason is that the long-wavelength surface waves do not bind to the surface and the grating structure strongly so that the scattering efficiency is not high. We later used a metasurface collimator, which was a combination of a second-order grating and subwavelength grooves (see Fig. 9(a)) [67], [68]. The latter have subwavelength spacing and depth. The optical power of the surface waves is trapped in the grooves so that the corrugations effectively reduce the plasma frequency and increase the skin depth. As a result, terahertz surface waves were much more strongly bound to the laser facet, so that the scattering efficiency by the second-order grating greatly increased. One can improve the confinement of the surface waves by more than one order of magnitude (from $\sim$300 μm for a planar GaAs-air interface to tens of micrometers for the metasurface collimator, see Fig. 9(c)). The collimated QCL showed 10-degree vertical divergence, and 19-degree lateral divergence (see Fig. 9(d)). There was no change to the lasing threshold current and maximum operating temperature (see Fig. 9(e)).

The subwavelength grooves right outside the laser aperture can be viewed as an optical analog to impedance matching circuits. They reduce the impedance mismatch between the waveguide mode and surface waves. Thus, the metasurface structure helps extract more power from the laser waveguide and couples a larger percentage of the output power into surface waves. This effect helps to alleviate the problem of poor power out-coupling of THz QCLs with double-metal waveguides. In the original unpatterned THz QCLs, the power reflectivity at the laser aperture is $\sim$90% due to a mismatch in propagation constant between the laser waveguide modes, $n_{\mathrm{wg}k_o}$ where $\mathrm{n_{wg}} \sim 3.5$, and the free space modes, $\mathrm{k_o}$. The spoof SPP grooves adjacent to the laser aperture support surface waves with increased propagation constant ($> \mathrm{k_o}$), representing a more efficient channel for power out-coupling. The grooves in the close vicinity of the laser aperture in Fig. 9(a) have a depth of 12 μm, giving rise to a propagation constant of $\sim 1.25\mathrm{k_o}$. As a result, 25% more power is extracted from the laser cavity, and $\sim$50% of all the emitted power is coupled into surface waves. We believe similar strategies can certainly be used for structures defined on an optical fiber facet.

IV. Patterning of Optical Fibers for Wavefront Control and Sensing

We have shown that the combination of plasmonics with the established platform of semiconductor lasers led to an interesting spectrum of possibilities, some of which may lead to useful applications. There are good reasons to believe that plasmonics and metasurfaces can also bring interesting opportunities to fiber optics: (1) Plasmonic and metasurface structures can have strong interactions with light, making it possible to create fiber optical devices with ultra-compact footprints. In particular, optical scatterers can be designed to interact with not only electric field but also magnetic field component of light; plasmonic structures or metasurfaces made of such scatterers can therefore control optical impedance (i.e., manipulate wavefront and maximize power transmission or reflection simultaneously) [37], [38]–[72]. (2) Optical losses can be minimized by using dielectric optical antennas as the building blocks. Mie resonances in optical scatterers made of high-refractive-index dielectric

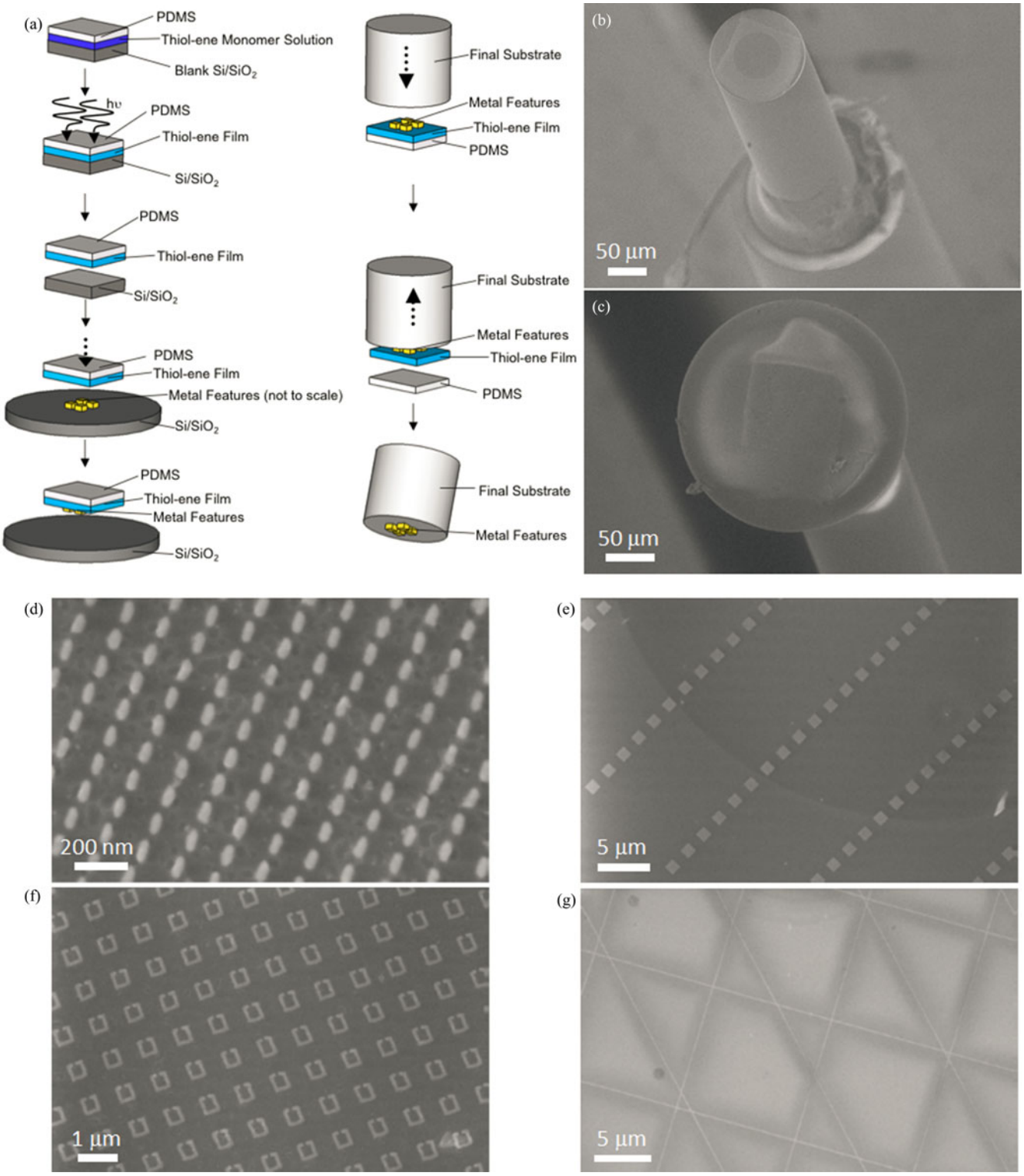

Fig. 10. (a) Schematic showing the procedure for transferring metallic nanostructures on to the facet of an optical fiber using the "decal transfer" technique. (b) SEM image of an optical fiber with its facet covered by an array of nanorods. (c) SEM image of a glass microsphere partially covered by an array of nanorods. (d) Zoom-in view of the nanorods defined on the microsphere. (e)–(g) Other nanostructures transferred on to fiber facets.

materials are just as versatile as plasmonic resonances in metallic scatterers [73]–[75]; they allow for controlling all properties of light, including amplitude, phase, polarization, wavevector, and optical impedance. (3) Plasmonic and metasurface structures can be patterned on the facets of optical fibers to intersect the guided modes or along the fibers (for example, on the exposed fiber cores) to interact with evanescent fields of the modes [76]–[78]. In the second scheme, the interaction between light

and designer nanostructures can be substantially enhanced because of the consecutive interaction between the two.

We have done some initial work on developing techniques to pattern optical fiber facets with nanostructures [79]–[81]. The size and shape of an optical fiber preclude the use of ordinary lithographic processes, because it is challenging to produce a coating of lithographic resist with uniform thickness. Focused ion beam (FIB) milling is not a good option: it is a slow sequential process, not scalable for high-volume fabrication; using FIB milling to define nanostructures directly on the facets of fibers also results in unintentional doping with gallium ions, which alter the optical response of the nanostructures [82].

A. "Decal Transfer" Technique

We have developed a "decal transfer" technique that allows for transferring of lithographically defined nanostructures on to the facets of optical fibers [79], [80]. Briefly, the process involves using an engineered sacrificial thiol-ene film to strip plasmonic antenna arrays from a substrate, transferring of the film and the antenna structures to a final substrate, and removing of the sacrificial film (see Fig. 10(a)). The essential component in the decal transfer technique is the engineered thiol-ene polymer, which is made of a mixture of commercially available chemicals, photocurable, and removable by oxygen plasma. The thiol groups in the polymer promote adhesion to gold nanostructures, so that the latter can be stripped off by the thiol-ene film from the Si/SiO_2 substrate. A stereoscope was used to align the final substrate over the plasmonic structures and make contact between the two. The final substrate can be functionalized with thiol groups to promote its adhesion to the plasmonic structures. Fig. 10(b) and (c) show successful transfer of gold nanorods to two final substrates that are almost impossible to pattern using conventional lithographic techniques: the facet of an optical fiber (125 μm in diameter), and a silica microsphere ($\sim$220 μm in diameter). Fig. 10(d) is a close-up of the nanorod array on the microsphere, showing minimal pattern distortion of the transferred array. The decal transfer technique can transfer a variety of dense, sparse, isolated or connected patterns (Figs. 10(e)–(g)).

We demonstrated a bidirectional optical fiber probe for the detection of surface-enhanced Raman scattering (SERS) signals [80] (see Fig. 11). In this application, arrays of metallic nanoantennas created by electron-beam lithography are transferred to the facets of optical fibers using the decal transfer technique. No adhesion layer was used and the antennas are held to the fiber facets by van der Waals forces. The coupled antennas in the array are designed to have a plasmonic resonance peaked at $\lambda = 650$ nm. The resonance is broad enough to provide enhancement for both the excitation light (He–Ne laser at $\lambda = 633$ nm) and the Raman signal of the analytes ($\lambda = 675 - 710$ nm). In experiments, we first prepared a self-assembled monolayer of benzenethiol on the gold antennas. The excitation light was coupled into the optical fiber from one facet. The light propagated to the facet decorated with the antenna array, excited the plasmonic resonance of the array, and generated a SERS signal from the benzenethiol monolayer adsorbed on the antenna

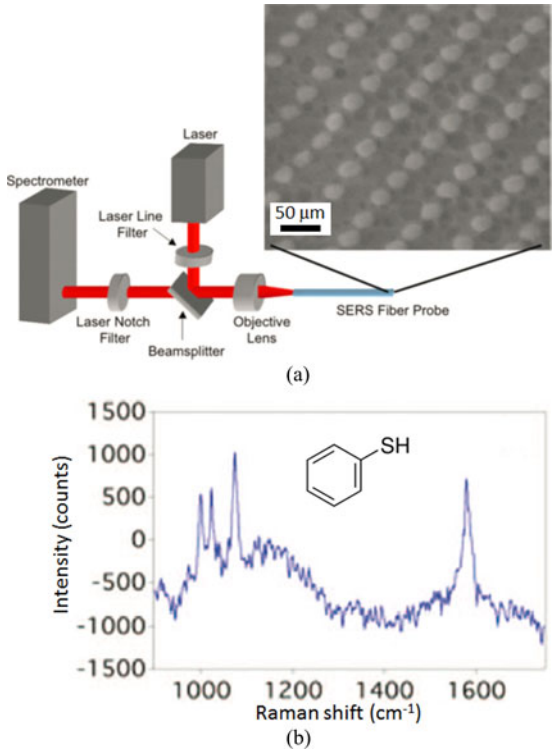

Fig. 11. (a) Schematic showing the experimental setup used to characterize the SERS optical fiber probe and an SEM image of an array of gold nanoantennas on the facet of a fiber. (b) Difference of the spectrum taken by the SERS probe and the spectrum taken from a fiber with a bare facet, showing the Raman spectrum of benzenethiol. Inset shows the molecular diagram of benzenethiol.

surface. The SERS signal propagated back through the fiber and was detected. By subtracting the spectrum taken from a fiber with a bare facet from that acquired from the SERS fiber probe, one got the Raman spectrum of benzenethiol, which has four vibrational modes at 995, 1020, 1075, and 1583 cm^{-1}. The enhancement factor (EF) of the SERS probe is estimated to be approximately $\times 10^5$. The EF is calculated by comparing the Raman signal per molecule generated in the SERS probe, and the Raman signal per molecule generated in liquid benzenethiol. This optical fiber SERS probe can be used for many different applications, such as sensing samples in remote locations, probing samples with small volumes, and performing in situ measurements.

B. "Nanoskiving" Technique

Another inexpensive and convenient method to create and transfer arrays of nanostructures to the cleaved facets of optical fibers is illustrated in Fig. 12(a) [81]. Large arrays of nanostructures (over 1 mm^2 in size) are created using the so-called "nanoskiving" technique [83]–[85], which is a combination of processes, including replica molding of high-aspect-ratio epoxy template, deposition of thin metal or dielectric films, and sectioning using an ultramicrotome. To be more specific, the fabrication process starts with a structured epoxy template, such as an array of pillars. The template is then coated with a metal film. Additional epoxy is added to fully encapsulate the metal

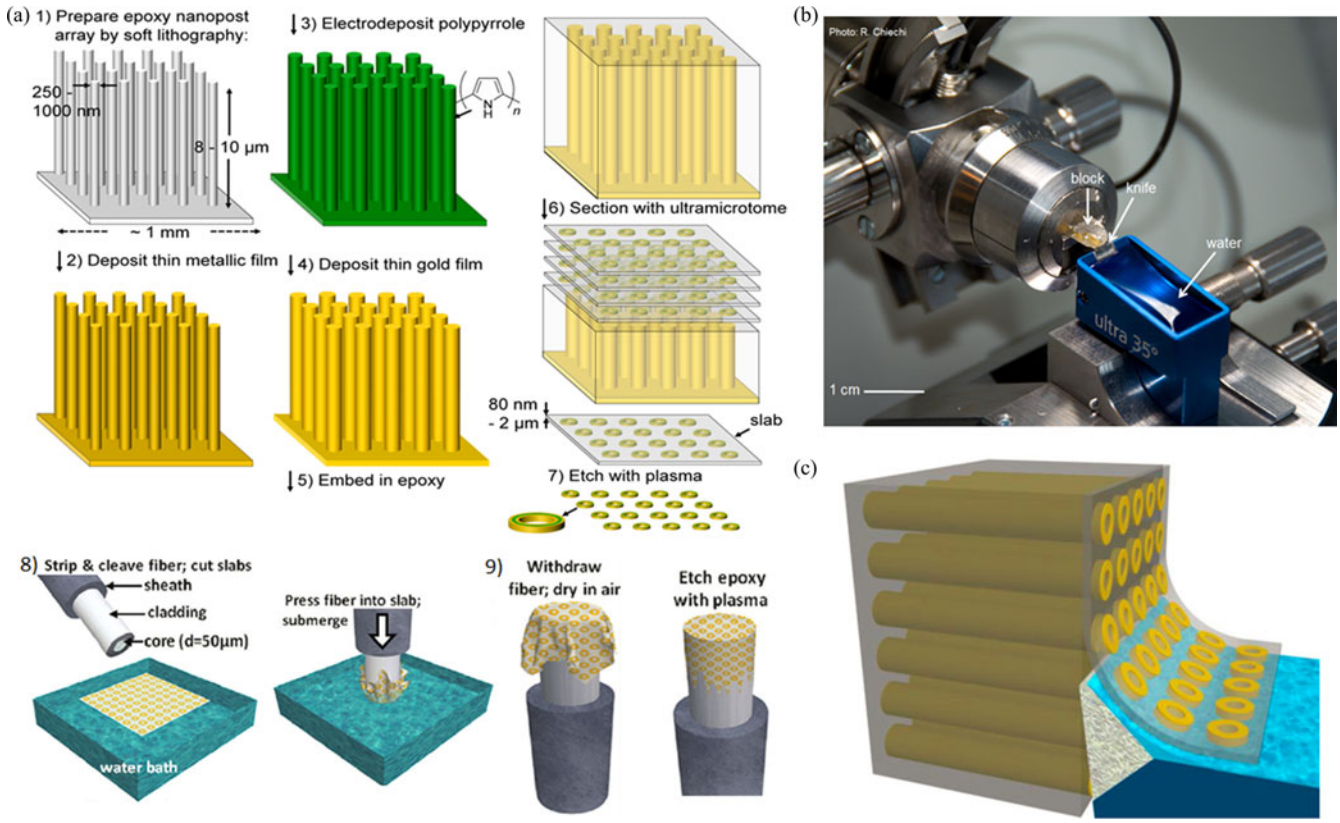

Fig. 12. (a) Procedure used to fabricate arrays of metallic nanostructures by embedding and sectioning a metallized array of epoxy nanopillars using an ultramicrotome, and procedure used to transfer arrays of metallic nanostructures to the facets of optical fibers. (b) Photograph of the sectioning head of an ultramicrotome. (c) Schematic showing the sectioning process.

film. The block of epoxy is mounted onto an ultramicrotome and is sectioned using a diamond knife. The process of "nanoskiving" produces arrays of nanostructures embedded in thin epoxy thin films. The latter are then transferred on to the facets of optical fibers. The epoxy embedding medium is later etched away, leaving the nanostructures deposited directly on the fiber facets.

The nanoskiving technique can be adapted to create a great variety of structures, many of which are beyond the fabrication capabilities of conventional lithographic techniques. Continuous metallic nanostructures can be produced if the epoxy template is conformally coated with the metal. Open-loop nanostructures can be fabricated if "shadow evaporation" is used to partially coat the template. Dielectric nanostructures can be created in the same way. Double patterning, which involves iterative transfers of thin epoxy films containing nanostructures, yields overlapping arrays of structures. High aspect-ratio nanostructures can be made by sectioning thick (up to a few micrometers) films from the epoxy block (see Fig. 13(a)). Arrays of nanostructures with a height gradient can be fabricated by tiling the epoxy block with respect to the diamond knife during the nanoskiving process (see Fig. 13(d)). Deposition using multiple source materials and subsequent embedding and sectioning could produce arrays of nanostructures made of multiple materials. For example, Fig. 13(b) shows fabricated arrays of crescents composed of silicon and silver. Nanoskiving is not limited to materials deposited using physical vapor deposition: semiconductor nanocrystals have been coated on the side walls of epoxy pillars and sectioned into arrays of nano-rings (see Fig. 13(c)); electrochemical growth and drop casting can add further compositional complexity to the final arrays of nanostructures.

Fig. 14(a) shows optical characterization of arrays of single rings and double concentric rings fabricated using nanoskiving and transferred onto a ZnSe substrate [85]. The transmission spectrum of the single rings exhibits a single dip, corresponding to the dipolar resonance of the ring; the spectrum of the double rings exhibits two dips. Fig. 14(b) shows an array of nanowires fabricated using nanoskiving and transferred onto a Si/SiO_2 substrate [83]. The wires are 2 μm in length and have a high aspect ratio: 10 nm in width and 100 nm in height. We illuminated the nanowire arrays with unpolarized white light at a large incident angle to minimize the background scattering from the substrate. The scattered light from the nanowires with polarizations perpendicular to the long axis of the nanowires was collected, because these scattered field components reveal the plasmonic resonance in the cross-section of the nanowires. Nanowires with different cross-sectional dimensions were fabricated: the width and height of the nanowires are controlled, respectively, by the thickness of the metal film and the microtome sectioning. For nanowires of the same width, the optical image and scattering spectra show a red shift with increasing nanowire height (see Figs. 14(c) and (d)).

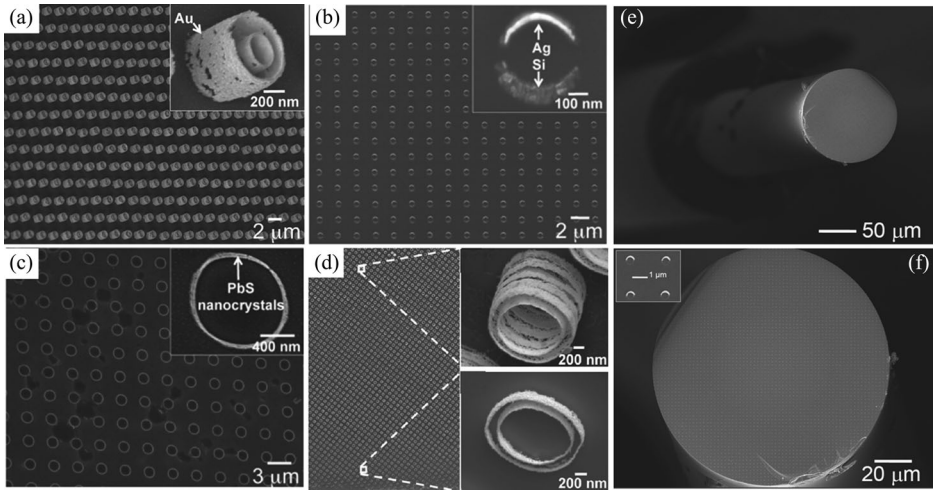

Fig. 13. (a)–(d) SEM images of two-dimensional arrays of nanostructures fabricated using the nanoskiving technique. (a) High-aspect-ratio concentric rings. (b) Counterfacing crescents of silver and silicon. (c) Microrings composed of PbS nanocrystals. (d) Concentric rings with a gradient of heights. (e) Arrays of gold crescents transferred on to a fiber facet. (f) Zoom-in view of (e).

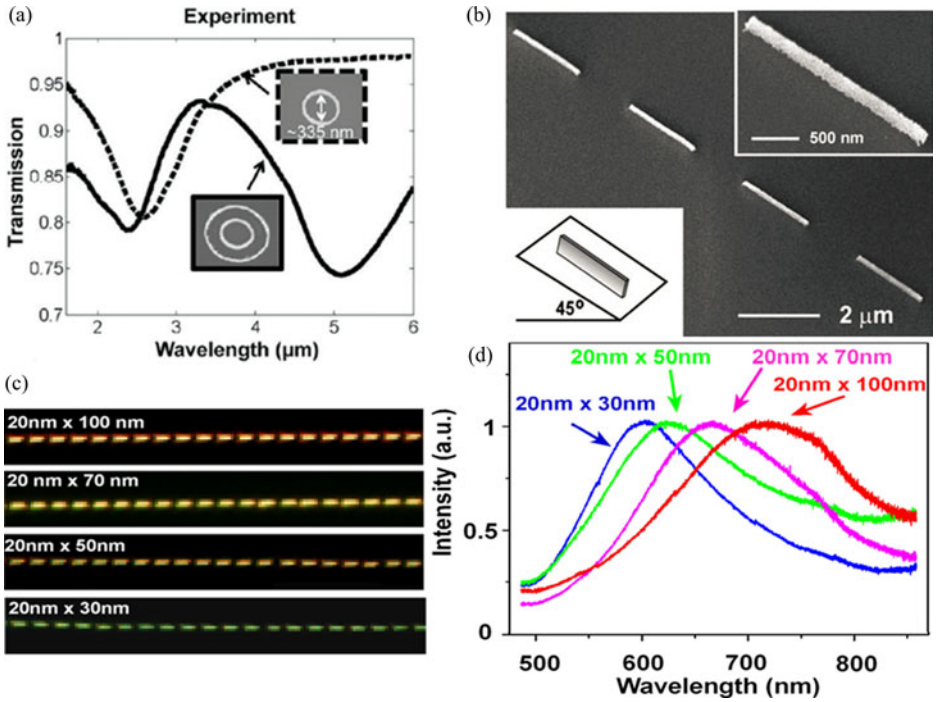

Fig. 14. (a) Transmission spectra for two types of arrays of gold nanorings patterned on a ZnSe substrate. (b) Gold nanowires with dimensions of approximately $2\ \mu\text{m} \times 10\ \text{nm} \times 100\ \text{nm}$. The insets show high-magnification image of one nanowire. (c) Dark-field optical images of gold nanowires having different dimensions (all 2-μm long). (d) Scattering spectra of gold nanowires in (c).

V. Conclusion

This paper discusses the basic concept of metasurfaces and various ways to implement the concept. The main features of metasurfaces are their ability to control all properties of light with subwavelength resolution, their small footprints, and the ease of fabrication. Such metasurfaces provide us with the unique possibility to fully control light with planar structures and thus realize "flat optics". The reduced dimensionality of optical metasurfaces opens up new physics and leads to novel device functionalities that are distinct from those achievable with bulk metamaterials.

The paper also discusses wavefront engineering of semiconductor lasers using flat designer plasmonic structures, and techniques to pattern arrays of nanostructures on optical fiber facets. The techniques we developed to couple laser emission into surface waves on the laser facets and to control such surface waves can be adapted to the fiber optics platform. The ability of patterning nanostructures on fiber facets or other small (flat or curved) surfaces will enable several applications, including sensing based on SERS, optical filtering, and diffraction gratings. The optical fiber platform could allow us to probe small volumes of samples or places hard to access (e.g.,

blood vessels). Nonconventional nanostructures, such as those with high aspect ratio and those consisting of two or more materials in the same plane, could enable studying of new physics and device functionalities.

ACKNOWLEDGEMENT

The authors would like to thank the contributions of Z. Gaburro, P. Genevet, M. A. Kats, F. Aieta, R. Blanchard, J. Lin, J.-P. Tetienne, G. Aoust, D. Sharma, T. S. Mansuripur, B. Gokden, S. J. Byrnes, J. Fan, Q. J. Wang, C. Pflügl, L. Diehl, E. J. Smythe, J. Bao, M. Kolle, N. Antoniou, Z. Yang, S. Ramanathan, M. Mumtaz Qazilbash, D. N. Basov, C. Ko, K. Fujita, T. Edamura, M. Yamanishi, H. Kan, S. P. Khanna, L. Li, A. G. Davies, E. H. Linfield, M. D. Dickey, D. J. Lipomi, R. V. Martinez, S. H. Kang, P. Kim, Q. Xu, R. M. Rioux, R. Perez-Castillejos, G. M. Whitesides, and J. Aizenberg to the research reviewed in this paper. Quantum cascade laser materials were provided by Hamamatsu Photonics KK.

REFERENCES

[1] A. J. Ward and J. B. Pendry, "Refraction and geometry in Maxwell's equations," *J. Modern Opt.*, vol. 43, pp. 773–793, 1996.
[2] U. Leonhardt, "Optical conformal mapping," *Science*, vol. 312, pp. 1777–1780, 2006.
[3] J. B. Pendry, D. Schurig, and D. R. Smith, "Controlling electromagnetic fields," *Science*, vol. 312, pp. 1780–1782, 2006.
[4] H. Chen, C. T. Chan, and P. Sheng, "Transformation optics and metamaterials," *Nature Mater.*, vol. 9, pp. 387–396, 2010.
[5] N. Yu, P. Genevet, M. A. Kats, F. Aieta, J.-P. Tetienne, F. Capasso, and Z. Gaburro, "Light propagation with phase discontinuities: Generalized laws of reflection and refraction," *Science*, vol. 334, pp. 333–337, 2011.
[6] N. Yu, P. Genevet, F. Aieta, M. A. Kats, R. Blanchard, G. Aoust, J.-P. Tetienne, Z. Gaburro, and F. Capasso, "Flat optics: Controlling wavefronts with optical antenna metasurfaces," *IEEE J. Sel. Topics Quantum Electron.*, vol. 19, no. 3, p. 4700423, May/Jun. 2013.
[7] N. Yu and F. Capasso, "Flat optics with designer metasurfaces," *Nature Mater.*, vol. 13, pp. 139–150, 2014.
[8] A. V. Kildishev, A. Boltasseva, and V. M. Shalaev, "Planar photonics with metasurfaces," *Science.*, vol. 339, art. no. 6125, 2013.
[9] C. L. Holloway, E. F. Kuester, J. A. Gordon, J. O'Hara, J. Booth, and D. R. Smith, "An overview of the theory and applications of metasurfaces: The two dimensional equivalents of metamaterials," *IEEE Antennas Propag. Mag.*, vol. 54, no. 2, pp. 10–35, Apr. 2012.
[10] P. Bharadwaj, B. Deutsch, and L. Novotny, "Optical antennas," *Adv. Opt. Photon.*, vol. 1, pp. 438–483, 2009.
[11] L. Novotny and N. van Hulst, "Antennas for light," *Nature Photon.*, vol. 5, pp. 83–90, 2011.
[12] Q. Zhao, J. Zhou, F. Zhang, and D. Lippens, "MIE resonance-based dielectric metamaterials," *Mater. Today*, vol. 12, no. 12, pp. 60–69, Dec. 2009.
[13] L. Liu, J. Sun, X. Fu, J. Zhou, Q. Zhao, B. Fu, J. Liao, and D. Lippens, "Artificial magnetic properties of dielectric metamaterials in terms of effective circuit model," *Progr. Electromagn. Res.*, vol. 116, pp. 159–170, 2011.
[14] J. A. Schuller, R. Zia, T. Taubner, and M. L. Brongersma, "Dielectric metamaterials based on electric and magnetic resonances of silicon carbide particles," *Phys. Rev. Lett.*, vol. 99, p. 107401, 2007.
[15] R. W. P. King, *The Theory of Linear Antennas*. Cambridge, MA, USA: Harvard Univ. Press, 1956.
[16] D. M. Pozar, S. D. Targonski, and H. D. Syrigos, "Design of millimeter wave microstrip reflectarrays," *IEEE Trans. Antenna Propag.*, vol. 45, no. 2, pp. 287–295, Feb. 1997.
[17] N. Gagnon, A. Petosa, and D. A. McNamara, "Research and development on phase-shifting surfaces," *IEEE Antennas Propag. Mag.*, vol. 55, no. 2, pp. 29–48, Apr. 2013.
[18] J. Huang and J. Encinar, *Reflectarray Antenna*. New York, NY, USA: Wiley, 2008.
[19] S. Uda, "Wireless beam of short electric waves (I)," *J. IEEE*, vol. 452, pp. 273–282, 1926.
[20] S. Uda, "Wireless beam of short electric waves (II)," *J. IEEE*, vol. 453, pp. 335–351, 1927.
[21] H. Yagi, "Beam transmission of the ultra short waves," *Proc. IRE*, vol. 16, p. 715–741, 1928.
[22] B. C. Kress and P. Meyrueis, *Digital Diffractive Optics: An Introduction to Planar Diffractive Optics and Related Technology*. New York, NY, USA: Wiley, 2000.
[23] S. Y. Chou, P. R. Krauss, and P. J. Renstrom, "Nanoimprint lithography," *J. Vac. Sci. Technol. B.*, vol. 14, pp. 4129–4133, 1996.
[24] Y. Xia and G. M. Whitesides, "Soft lithography," *Angewandte Chemie*, vol. 37, pp. 550–575, 1998.
[25] B. J. Lin, "Deep UV lithography," *J. Vacuum Sci. Technol.*, vol. 12, pp. 1317–1320, 1975.
[26] M. Totzeck, W. Ulrich, A. Göhnermeier, and W. Kaiser, "Semiconductor fabrication: Pushing deep ultraviolet lithography to its limits," *Nature Photon.*, vol. 1, pp. 629–631, 2007.
[27] F. Aieta, P. Genevet, N. Yu, M. A. Kats, Z. Gaburro, and F. Capasso, "Out-of-plane reflection and refraction of light by anisotropic optical antenna metasurfaces with phase discontinuities," *Nano Lett.*, vol. 12, pp. 1702–1706, 2012.
[28] Y. Svirko, N. Zheludev, and M. Osipov, "Layered chiral metallic microstructures with inductive coupling," *Appl. Phys. Lett.*, vol. 78, pp. 498–500, 2001.
[29] R. Blanchard, G. Aoust, P. Genevet, N. Yu, M. A. Kats, Z. Gaburro, and F. Capasso, "Modeling nanoscale V-shaped antennas for the design of optical phased arrays," *Phys. Rev. B.,* vol. 85, p. 155457, 2012.
[30] M. A. Kats, P. Genevet, G. Aoust, N. Yu, R. Blanchard, F. Aieta, Z. Gaburro, and F. Capasso, "Giant birefringence in optical antenna arrays with widely tailorable optical anisotropy," *Proc. Nat. Academy Sci. USA*, vol. 109, pp. 12364–12368, 2012.
[31] M. A. Kats, N. Yu, P. Genevet, Z. Gaburro, and F. Capasso, "Effect of radiation damping on the spectral response of plasmonic components," *Opt. Exp.*, vol. 22, pp. 21748–21753, 2011.
[32] X. Ni, N. K. Emani, A. V. Kildishev, A. Boltasseva, and V. M. Shalaev, "Broadband light bending with plasmonic nanoantennas," *Science*, vol. 335, p. 427, 2012.
[33] S. Sun, K.-Y. Yang, C.-M. Wang, T.-K. Juan, W. T. Chen, C. Y. Liao, Q. He, S. Xiao, W.-T. Kung, G.-Y. Guo, L. Zhou, and D. P. Tsai, "High-efficiency broadband anomalous reflection by gradient meta-surfaces," *Nano Lett.*, vol. 12, pp. 6223–6229, 2012.
[34] S. Sun, Q. He, S. Xiao, Qin Xu, X. Li, and L. Zhou, "Gradient-index meta-surfaces as a bridge linking propagating waves and surface waves," *Nature Mater.*, vol. 11, pp. 426–431, Apr. 2012.
[35] F. Aieta, P. Genevet, M. A. Kats, N. Yu, R. Blanchard, Z. Gaburro, and F. Capasso, "Aberration-free ultra-thin flat lenses and axicons at telecom wavelengths based on plasmonic metasurfaces," *Nano Lett.*, vol. 12, pp. 4932–4936, 2012.
[36] F. Aieta, P. Genevet, M. Kats, and F. Capasso, "Aberrations of flat lenses and aplanatic metasurfaces," *Opt. Exp.*, vol. 21, pp. 31530–31539, 2013.
[37] F. Monticone, N. M. Estakhri, and A. Alù, "Full control of nanoscale optical transmission with a composite metascreen," *Phys. Rev. Lett.*, vol. 110, p. 203903, 2013.
[38] C. Pfeiffer and A. Grbic, "Metamaterial Huygens' surfaces: Tailoring wave fronts with reflectionless sheets," *Phys. Rev. Lett.*, vol. 110, p. 197401, 2013.
[39] N. Yu, F. Aieta, P. Genevet, M. A. Kats, Z. Gaburro, and F. Capasso, "A broadband, background-free quarter-wave plate based on plasmonic metasurfaces," *Nano Lett.*, vol. 12, pp. 6328–6333, 2012.
[40] J. F. Nye and M. V. Berry, Dislocations in wave trains," *Proc. R. Soc. Lond. A*, vol. 336, pp. 165–190, Jan. 1974.
[41] M. Padgett, J. Courtial, and L. Allen, "Light's orbital angular momentum," *Phys. Today*, vol. 57, pp. 35–40, May 2004.
[42] P. Genevet, N. Yu, F. Aieta, J. Lin, M. A. Kats, R. Blanchard, M. O. Scully, Z. Gaburro, and F. Capasso, "Ultra-thin plasmonic optical vortex plate based on phase discontinuities," *Appl. Phys. Lett.*, vol. 100, p. 13101, 2012.
[43] S. Pancharatnam, "Generalized theory of interference, and its applications: Part I—Coherent pencils," *Proc. Indian Acad. Sci. Sect. A*, vol. 44, pp. 247–262, 1956.
[44] M. V. Berry, "Quantal phase factors accompanying adiabatic changes," *Proc. R. Soc. London A*, vol. 392, pp. 45–57 1984.

[45] M. Kang, T. Feng, H.-T. Wang, and J. Li, "Wave front engineering from an array of thin aperture antennas," *Opt. Exp.*, vol. 14, pp. 15882–15890, Jul. 2012.
[46] Z. Bomzon, V. Kleiner, and E. Hasman, "Computer-generated space-variant polarization elements with subwavelength metal stripes," *Opt. Lett.*, vol. 26, pp. 33–35, 2001.
[47] Z. Bomzon, G. Biener, V. Kleiner, and E. Hasman, "Space-variant Pancharatnam–Berry phase optical elements with computer-generated subwavelength gratings," *Opt. Lett.*, vol. 27, pp. 1141–1143, 2002.
[48] E. Hasman, V. Kleiner, G. Biener, and A. Niv, "Polarization dependent focusing lens by use of quantized Pancharatnam–Berry phase diffractive optics," *Appl. Phys. Lett.*, vol. 82, pp. 328–330, Jan. 2003.
[49] N. Shitrit, I. Bretner, Y. Gorodetski, V. Kleiner, and E. Hasman, "Optical spin hall effects in plasmonic chains," *Nano Lett.*, vol. 11, pp. 2038–2042, Apr. 2011.
[50] L. Huang, X. Chen, H. Mühlenbernd, G. Li, B. Bai, Q. Tan, G. Jin, T. Zentgraf, and S. Zhang, "Dispersionless phase discontinuities for controlling light propagation," *Nano. Lett.*, vol. 12, pp. 5750–5755, Oct. 2012.
[51] D. Lin, P. Fan, E. Hasman, and M. L. Brongersma, "Dielectric gradient metasurface optical elements," *Science*, vol. 345, pp. 298–302, 2014.
[52] J. Lin, P. Genevet, M. A. Kats, N. Antoniou, and F. Capasso, "Nanostructured holograms for broadband manipulation of vector beams," *Nano Lett.*, vol. 13, pp. 4269–4274, 2013.
[53] M. A. Kats, D. Sharma, J. Lin, P. Genevet, R. Blanchard, Z. Yang, M. Mumtaz Qazilbash, D. N. Basov, S. Ramanathan, and F. Capasso, "Ultra-thin perfect absorber employing a tunable phase change material," *Appl. Phys. Lett.*, vol. 101, p. 221101, 2012.
[54] M. A. Kats, S. J. Byrnes, R. Blanchard, M. Kolle, P. Genevet, J. Aizenberg, and F. Capasso, "Enhancement of absorption and color contrast in ultra-thin highly absorbing optical coatings," *Appl. Phys. Lett.*, vol. 103, p. 101104, 2013.
[55] M. A. Kats, R. Blanchard, P. Genevet, and F. Capasso, "Nanometre optical coatings based on strong interference effects in highly absorbing media," *Nature Mater.*, vol. 12, pp. 20–24, 2013.
[56] M. M. Qazilbash, M. Brehm, B.-G. Chae, P.-C. Ho, G. O. Andreev, B.-J. Kim, S. J. Yun, A. V. Balatsky, M. B. Maple, F. Keilmann, H.-T. Kim, and D. N. Basov, "Mott transition in VO_2 revealed by infrared spectroscopy and nano-imaging," *Science*, vol. 318, pp. 1750–1753, 2007.
[57] M. A. Kats, R. Blanchard, S. Zhang, P. Genevet, C. Ko, S. Ramanathan, and F. Capasso, "Vanadium dioxide as a natural disordered metamaterial: Perfect thermal emission and large broadband negative differential thermal emittance," *Phys. Rev.*, vol. X3, p. 41004, 2013.
[58] N. Yu, R. Blanchard, J. Fan, Q. J. Wang, C. Pflügl, L. Diehl, T. Edamura, M. Yamanishi, H. Kan, and F. Capasso, "Plasmonics for laser beam shaping," *IEEE Trans. Nanotechnol.*, vol. 9, no. 1, pp. 11–29, Feb. 2010.
[59] N. Yu, Q. J. Wang, and F. Capasso, "Beam engineering of quantum cascade lasers," *Laser Photon. Rev.*, vol. 6, no. 1, p. 24–46, 2012.
[60] N. Yu, E. Cubukcu, L. Diehl, M. A. Belkin, K. B. Crozier, D. Bour, S. Corzine, G. Höfler, and F. Capasso, "Plasmonic quantum cascade laser antenna," *Appl. Phys. Lett.*, vol. 91, p. 173113, 2007.
[61] N. Yu, E. Cubukcu, L. Diehl, D. Bour, S. Corzine, J. Zhu, G. Höfler, yes K. B. Crozier, and F. Capasso, "Bowtie plasmonic quantum cascade laser antenna," *Opt. Exp.*, vol. 15, pp. 13272–13281, 2007.
[62] N. Yu, J. Fan, Q. J. Wang, C. Pflügl, L. Diehl, T. Edamura, M. Yamanishi, H. Kan, and F. Capasso, "Small-divergence semiconductor lasers by plasmonic collimation," *Nature Photon.*, vol. 2, pp. 564–570, 2008
[63] N. Yu, R. Blanchard, J. Fan, T. Edamura, M. Yamanishi, H. Kan, and F. Capasso, "Small divergence semiconductor lasers with two-dimensional plasmonic collimators," *Appl. Phys. Lett.*, vol. 93, p. 181101, 2008.
[64] N. Yu, R. Blanchard, J. Fan, Q. J. Wang, C. Pflügl, L. Diehl, T. Edamura, M. Yamanishi, H. Kan, and F. Capasso, "Quantum cascade lasers with integrated plasmonic antenna-array collimators," *Opt. Exp.*, vol. 16, pp. 19447–19461, 2008.
[65] N. Yu, Q. J. Wang, C. Pflügl, L. Diehl, T. Edamura, M. Yamanishi, H. Kan, and F. Capasso, "Semiconductor lasers with integrated plasmonic polarizers," *Appl. Phys. Lett.*, vol. 94, p. 151101, 2009.
[66] N. Yu, M. A. Kats, C. Pflügl, M. Geiser, Q. J. Wang, M. A. Belkin, F. Capasso, M. Fischer, A. Wittmann, J. Faist, T. Edamura, S. Furuta, M. Yamanishi, and H. Kan, "Multi-beam multi-wavelength semiconductor lasers," *Appl. Phys. Lett.*, vol. 95, p. 161108, 2009.
[67] N. Yu, Q. J. Wang, M. A. Kats, J. A. Fan, S. P. Khanna, L. Li, A. G. Davies, E. H. Linfield, and F. Capasso, "Designer spoof-surface-plasmon structures collimate terahertz laser beams," *Nature Mater.*, vol. 9, pp. 730–735, 2010.
[68] N. Yu, Q. J. Wang, M. A. Kats, J. A. Fan, F. Capasso, S. P. Khanna, L. Li, A. G. Davies, and E. H. Linfield, "Terahertz plasmonics," *Electron. Lett.*, vol. 46, pp. s52–s57, 2010.
[69] J.-P. Tetienne, R. Blanchard, N. Yu, P. Genevet, M. A. Kats, J. A. Fan, T. Edamura, S. Furuta, M. Yamanishi, and F. Capasso, "Dipolar modeling and experimental demonstration of multi-beam plasmonic collimators," *New J. Phys.*, vol. 13, p. 53057, 2011.
[70] R. Blanchard, T. S. Mansuripur, B. Gokden, N. Yu, M. A. Kats, P. Genevet, K. Fujita, T. Edamura, M. Yamanishi, and F. Capasso, "High-power low-divergence tapered quantum cascade lasers with plasmonic collimators," *Appl. Phys. Lett.*, vol. 102, p. 191114, 2013.
[71] S. Fathololoumi, E. Dupont, C. W. I. Chan, Z. R. Wasilewski, S. R. Laframboise, D. Ban, A. Mátyás, C. Jirauschek, Q. Hu, and H. C. Liu, "Terahertz quantum cascade lasers operating up to $\sim$200 K with optimized oscillator strength and improved injection tunneling," *Opt. Exp.*, vol. 20, pp. 3866–3876, 2012.
[72] G. Gok and A. Grbic, "Tailoring the phase and power flow of electromagnetic fields," *Phys. Rev. Lett.*, vol. 111, p. 233904, 2013.
[73] A. B. Evlyukhin, S. M. Novikov, U. Zywietz, R. L. Eriksen, C. Reinhardt, S. I. Bozhevolnyi, and B. N. Chichkov, "Demonstration of magnetic dipole resonances of dielectric nanospheres in the visible region," *Nano Lett.*, vol. 12, pp. 3749–3755, 2012.
[74] I. Staude, A. E. Miroshnichenko, M. Decker, N. T. Fofang, S. Liu, E. Gonzales, J. Dominguez, T. S. Luk, D. N. Neshev, I. Brener, and Y. Kivshar, "Tailoring directional scattering through magnetic and electric resonances in subwavelength silicon nanodisks," *ACS Nano*, vol. 7, pp. 7824–7832, 2013.
[75] Y. Yang, W. Wang, P. Moitra, I. I. Kravchenko, D. P. Briggs, and J. Valentine, "Dielectric meta-reflectarray for broadband linear polarization conversion and optical vortex generation," *Nano Lett.*, vol. 14, pp. 1394–1399, 2014.
[76] S. Kang, H.-E. Joe, J. Kim, Y. Jeong, B.-K. Min, and K. Oh, "Subwavelength plasmonic lens patterned on a composite optical fiber facet for quasi-one-dimensional Bessel beam generation," *Appl. Phys. Lett.*, vol. 98, p. 241103, 2011.
[77] X. Yu, D. Yong, H. Zhang, H. Li, Y. Zhang, C. C. Chan, H.-P. Ho, H. Liu, and D. Liu, "Plasmonic enhanced fluorescence spectroscopy using side-polished microstructured optical fiber," *Sens. Actuators*, vol. B 160, pp. 196–201, 2011.
[78] B. Lee, S. Roh, and J. Park, "Current status of micro- and nano-structured optical fiber sensors," *Opt. Fiber Technol.*, vol. 15, pp. 209–221, 2009.
[79] E. J. Smythe, M. D. Dickey, G. M. Whitesides, and F. Capasso, "A technique to transfer metallic nanoscale patterns to small and non-planar surfaces," *ACS Nano*, vol. 3, pp. 59–65, 2009.
[80] E. J. Smythe, M. D. Dickey, J. Bao, G. M. Whitesides, and F. Capasso, "Optical antenna arrays on a fiber facet for in situ surface-enhanced Raman scattering detection," *Nano Lett.*, vol. 9, pp. 1132–1138, 2009.
[81] D. J. Lipomi, R. V. Martinez, M. A. Kats, S. H. Kang, P. Kim, J. Aizenberg, F. Capasso, and G. M. Whitesides, "Patterning the tips of optical fibers with metallic nanostructures using nanoskiving," *Nano Lett.*, vol. 11, no. 2, pp. 632–636, 2010.
[82] Y. Q. Fu and N. K. A. Bryan, "Investigation of physical properties of quartz after focused ion beam bombardment," *Appl. Phys. B, Lasers Opt.*, vol. 80, no. 4–5, pp. 581–585, 2005.
[83] Q. Xu, J. Bao, F. Capasso, and G. M. Whitesides, "Surface plasmon resonances of free-standing gold nanowires fabricated by nanoskiving," *Angewandte Chemie*, vol. 118, pp. 3713–3717, 2006.
[84] Q. Xu, J. Bao, R. M. Rioux, R. Perez-Castillejos, F. Capasso, and G. M. Whitesides, "Fabrication of large-area patterned nanostructures for optical applications by nanoskiving," *Nano Lett.*, vol. 7, pp. 2800–2805, 2007.
[85] D. J. Lipomi, M. A. Kats, P. Kim, S. H. Kang, J. Aizenberg, F. Capasso, and G. M. Whitesides, "Fabrication and replication of arrays of single or multicomponent nanostructures by replica molding and mechanical sectioning," *ACS Nano*, vol. 4, pp. 4017–4726, 2010.

Nanfang Yu received the Ph.D. degree in engineering sciences from Harvard University, Cambridge, MA, USA, in 2009, and the B.S. degree in electronics from the Department of Electronics, Peking University, Beijing, China, in 2004. He is an Assistant Professor of Applied Physics at the Department of Applied Physics and Applied Mathematics, Columbia University. He was a Research Associate in the School of Engineering and Applied Sciences, Harvard University during 2009 and 2012. His research interests include nanophotonics and device physics. His research group conducts experimental work on plasmonics, metamaterials, and mid-infrared and terahertz optoelectronic devices.

Dr. Yu has published more than 30 articles in peer-reviewed scientific journals, including *Science*, *Physical Review Letters*, *Nature Materials*, and *Nature Photonics*.

Federico Capasso is the Robert Wallace Professor of applied physics at Harvard University, Cambridge, MA, USA, which he joined in 2003 after a 27 years career at Bell Labs, where he did research, became Bell Labs Fellow, and held several management positions including the Vice-President for Physical Research. His research has spanned basic science and applications in the areas of electronics, photonics, nanoscale science and technology including plasmonics, metasurfaces, and the Casimir effect. He pioneered bandstructure engineering of artificially structured materials and devices and invented the quantum cascade laser. He performed the first measurement of the repulsive Casimir force. He and his group recently discovered powerful generalizations of the laws of reflection and refraction applicable to metasurfaces and demonstrated that the latter can be used to design new planar optical components (flat optics). He is a Member of the National Academy of Sciences, the National Academy of Engineering, a fellow of the American Academy of Arts and Sciences. His awards include the King Faisal International Prize for Science, the American Physical Society Arthur Schawlow Prize, the Wetherill Medal of the Franklin Institute, the IEEE Edison Medal, the SPIE Gold Medal, the European Physical Society Quantum Electronics Prize; the Berthold Leibinger Zukunftspreis (the future prize), the Julius Springer Prize for Applied Physics, the Jan Czochralski Award of the European Material Research Society for lifetime achievements in Materials Science; the IEEE D. Sarnoff Award in Electronics, the IEEE/LEOS William Streifer Award, the Optical Society of America Robert Wood prize, the Rank Prize in Optoelectronics, the Material Research Society Medal, the Welker Medal, the Duddell Medal and Prize of the Institute of Physics (UK), the Newcomb Cleveland Prize of the American Association for the Advancement of Science, the "Vinci of Excellence" LMVH Prize and the New York Academy of Sciences Award.